Original papers
Advanced structural materials, materials for extreme conditions

УДК 621.791.13 DOI: 10.17277/jamt-2026-11-02-104-117

Study of evolution and phase formation at the 08Cr18Ni10Ti–AlMg6 weld interface after explosive welding and heat treatment via layer-by-layer XRD analysis

© Andrey Yu. Malakhov[a], Dmitry Yu. Kovalev[a], Stepan A. Seropyan[a]✉, Nemat N. Niyozbekov[a], Igor V. Denisov[a], Gulnaz R. Saikova[a]

[a] *Merzhanov Institute of Structural Macrokinetics and Materials Science, Russian Academy of Science, 8, Academician Osipyan St., Chernogolovka, 142432, Russian Federation*

✉ stepan.seropyan@yandex.ru

Abstract. The phase evolution in the joint zone of the 08Cr18Ni10Ti–AlMg6 bimetal obtained by explosive welding followed by isothermal annealing at 500–550 °C was investigated using the method of layer-by-layer XRD analysis. It was established that after explosive welding, a metastable quasicrystalline phase, $Al_{86}Fe_{14}$, forms in the near-surface layers. This phase decomposes during isothermal annealing, leading to the formation of equilibrium intermetallic compounds Al_5Fe_2 and $Al_{13}Fe_4$. Additionally, after annealing, the formation of a ternary phase, $Cr_2Mg_3Al_{18}$, is detected, indicating the activation of diffusion interaction between the components of the steel and the aluminium alloy. Thus, a sequential evolution of the phase composition in the joint zone after explosive welding and thermal exposure is demonstrated. The results obtained expand the understanding of the mechanisms of phase formation and diffusion processes at the joint interface in the 08Cr18Ni10Ti–AlMg6 bimetal during explosive welding, as well as the influence of thermal exposure on phase evolution.

Keywords: explosive welding; phase transformation; 08Cr18Ni10Ti steel; AlMg6 alloy; layer-by-layer XRD; recrystallization.

For citation: Malakhov AYu, Kovalev DYu, Seropyan SA, Niyozbekov NN, Denisov IV, Saikova GR. Study of evolution and phase formation at the 08Cr18Ni10Ti–AlMg6 weld interface after explosive welding and heat treatment via layer-by-layer XRD analysis. *Journal of Advanced Materials and Technologies*. 2026;11(2):104-117. DOI: 10.17277/jamt-2026-11-02-104-117

Исследование эволюции и фазообразования на границе раздела сварного соединения 08Х18Н10Т–АМг6 после сварки взрывом и термической обработки с помощью послойного рентгеноструктурного анализа

© А. Ю. Малахов[a], Д. Ю. Ковалев[a], С. А. Серопян[a]✉, И. В. Денисов[a], Н. Н. Ниезбеков[a], Г. Р. Сайкова[a]

[a] *Институт структурной макрокинетики и проблем материаловедения им. А. Г. Мержанова РАН, ул. Академика Осипьяна, 8, Черноголовка, 142432, Российская Федерация*

✉ stepan.seropyan@yandex.ru

Аннотация. Методом послойного рентгеноструктурного анализа (РФА) исследована фазовая эволюция в зоне соединения биметалла сталь 08Х18Н10Т–АМг6, полученного сваркой взрывом, с последующим изотермическим отжигом при 500–550 °С. Установлено, что после сварки взрывом в приповерхностных слоях формируется метастабильная квазикристаллическая фаза $Al_{86}Fe_{14}$, которая распадается при изотермическом отжиге с образованием равновесных интерметаллических соединений Al_5Fe_2 и $Al_{13}Fe_4$. Также после отжига фиксируется формирование тройной фазы $Cr_2Mg_3Al_{18}$, что свидетельствует об активизации диффузионного взаимодействия компонентов стали и алюминиевого сплава. Таким образом, показана последовательная эволюция фазового состава в зоне соединения после сварки взрывом и термического воздействия. Полученные результаты расширяют представления о механизмах фазообразования и диффузионных процессов на границе соединения в биметалле сталь 08Х18Н10Т–АМг6 при сварке взрывом, а также о влиянии термического воздействия на эволюцию фаз.

Ключевые слова: сварка взрывом; фазовое изменение; сталь 08Х18Н10Т; сплав АМг6; послойный РФА; рекристаллизация.

Для цитирования: Malakhov AYu, Kovalev DYu, Seropyan SA, Niyozbekov NN, Denisov IV, Saikova GR. Study of evolution and phase formation at the 08Cr18Ni10Ti–AlMg6 weld interface after explosive welding and heat treatment via layer-by-layer XRD analysis. *Journal of Advanced Materials and Technologies*. 2026;11(2):104-117. DOI: 10.17277/jamt-2026-11-02-104-117

1. Introduction

Aluminium alloys are widely used in aircraft, mechanical engineering, marine construction and the chemical industry [1]. For example, aluminium-magnesium (Al–Mg) alloys are used due to their high corrosion resistance, low density and high strength [2–4]. At present, bimetallic transition joints consisting of Al–Mg alloy and stainless steel enable weight reduction in various structures [5, 6]. The bimetallic transitions have significant potential for transport equipment and large-scale chemical vessel production [7, 8]. These transitions are produced by using friction stir welding [9], cold rolling [10], gas tungsten arc welding [11], spot welding [12], diffusion welding [13], explosive welding (EW) [14], and magnetic pulse welding [15]. In contrast to other methods, EW enables the joining of large-area plates without requiring complex high-cost equipment [16, 17]. Welding Al–Mg alloys to steels presents many challenges, inherent in all welding methods. Primarily, there is a significant difference in thermophysical properties between the Al–Mg alloys and steels [18].

Furthermore, the formation of a strong joint is complicated by: 1) the accumulation of Mg near the weld interface, 2) the presence of MgO on the Al–Mg alloy surface [19], and 3) the formation of brittle Fe–Al intermetallic compounds resulting from the low solubility of Mg atoms in Fe [20–22]. These factors are important to consider when plastic deformation occurs in EW [16, 23]. There are numerous scientific works that have investigated phase formation between Fe and Al [25–27]. These works show that Al_3Fe and Al_5Fe_2 are the dominant phases.

One of the methods for reducing Fe–Al intermetallic compounds at the weld interface involves using interlayers (e.g., Ti, Cu, Al, Ta) [24]. However, using interlayers may not prevent the formation of brittle Fe–Al intermetallic compounds during service [16].

Chemical composition of the intermetallic compounds at the weld interface is primarily analyzed on cross-sectional planes [19]. However, isolated particles and intermetallic compounds with low concentrations cannot be detected by this method.

This study investigates phase formation at the AlMg6 alloy–08Cr18Ni10Ti steel weld interface via layer-by-layer X-ray diffraction (XRD) analysis with sequential layer removal. Thus, this study enabled high-accuracy detection of low-concentration intermetallic compounds at significant distances from the weld interface.

2. Materials and Methods

2.1. Materials

Initial materials included aluminium-magnesium alloy AlMg6 sheet (4×200×300 mm) and 08Cr18Ni10Ti stainless steel sheet (3×200×300 mm). Their chemical compositions are given in Table 1.

2.2. The basic setup for the EW experiment

Prior to the start of the experiment, the initial sheets were cleaned from the oxide films and rusts. Figure 1 shows the basic setup for the EW experiment. The explosive used is a mixture of microporous ammonium nitrate and diesel oil (ANFO) at the ratio 96:4. The detonation velocity was 2500 m·s^{-1}. The distance between the flyer and base sheets was 6 mm. For other details of the EW experiments, see [28]. The EW parameters were calculated using the formulas in [29].

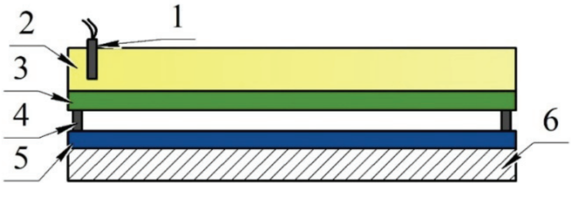

Fig. 1. Basic setup for explosive welding: *1* – detonator; *2* – explosive; *3* – flyer sheet (08Cr18Ni10Ti steel); *4* – support; *5* – base sheet (AlMg6 alloy); *6* – anvil (low carbon steel)

Table 1. Chemical compositions (wt. %) of initial materials

Material	Element (wt. %)									
	Fe	Si	C	Ti	Al	Mg	Cu	Cr	Ni	Mn
AlMg6 (Russian Standard 4784-2019)	0.4	0.4	–	0.1	Base	5.8–6.8	0.1	–	–	0.5–0.8
08Cr18Ni10Ti (Russian Standard 5632-2014)	Base	0.8	0.08	1.0	–	–	0.3	17–19	9–11	2.0

2.3. XRD analysis

Specimens for XRD analysis were prepared following the methodology illustrated in Fig. 2*a*. The wire cutting machine DK7725 was used to cut the specimens. Specimens were heat-treated in air at 500 and 550 °C for holding times of 60, 90, and 120 min, respectively. The specimens were split after EW and heat treatment (Fig. 2*b*). The surfaces of the split specimens were analyzed using XRD analysis.

The XRD analysis of the specimens was performed before and after the EW. On an automated LAP-1000 grinding/polishing machine, a layer of (30 ± 5) μm was removed from the analysis surface of AlMg6 and 08Cr18Ni10Ti in two stages, with approximately (15 ± 5) μm removed per stage, followed by XRD analysis (Fig. 3). Heat treated specimens underwent the same procedure: grinding (15 ± 5) μm → XRD → repeat → total removal: (30 ± 5) μm.

3. Results and Discussion

3.1. Analysis of initial materials before explosive welding

The diffraction pattern from the initial surface (pre-explosive welding) of 08Cr18Ni10Ti steel reveals two phases – austenite and ferrite (Fig. 4). A pronounced {220} austenite texture is observed, evidently resulting from prior rolling. The microstructure further indicates highly elongated grains.

The diffraction pattern from the initial surface of the AlMg6 alloy (Fig. 5) reveals that the primary phase is an aluminium-based FCC solid solution

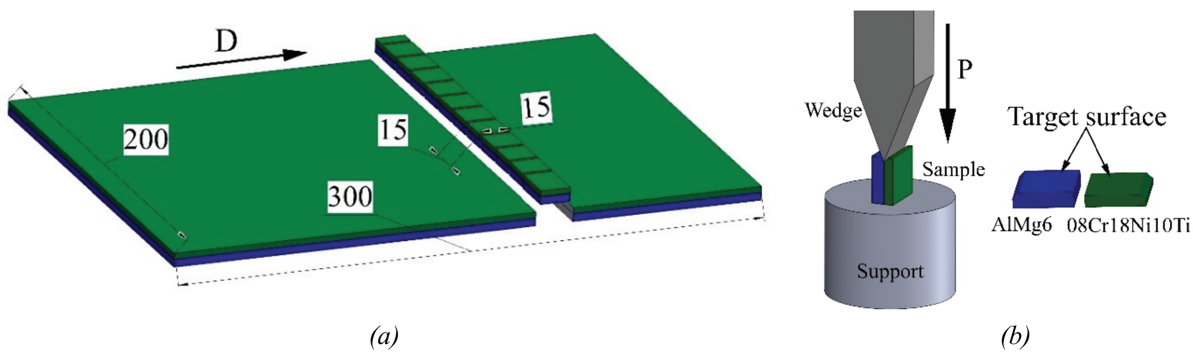

Fig. 2. Specimen preparation:
a – specimen extraction; *b* – layer separation method; *D* – detonation direction; *P* – applied pressure direction

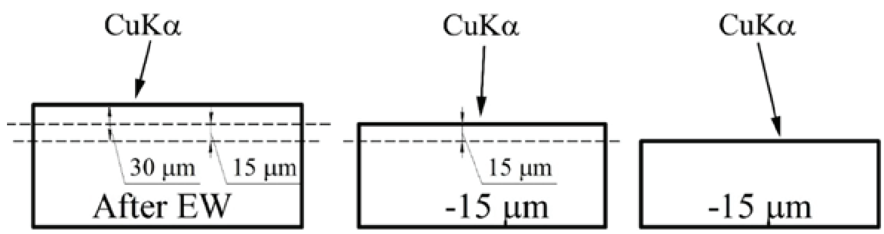

Fig. 3. Schematic of stepwise layer removal

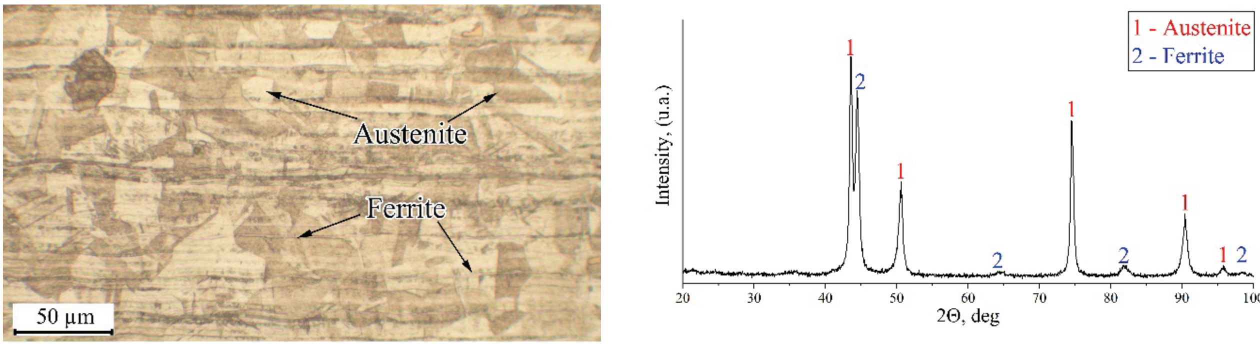

(a) *(b)*

Fig. 4. Microstructure of 08Cr18Ni10Ti steel with XRD pattern

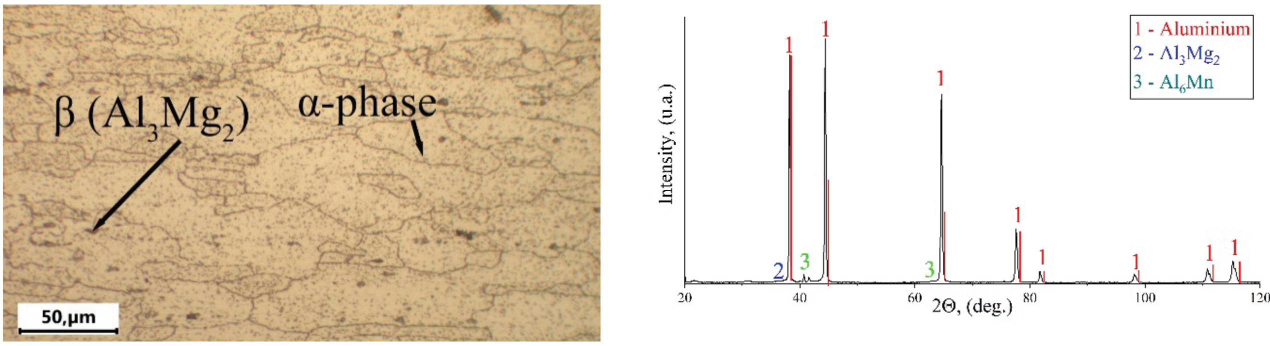

(a) *(b)*

Fig. 5. Microstructure of AlMg6 alloy with XRD pattern

(α-phase). Reflections of the solid solution are shifted relative to pure aluminium angular positions, indicating dissolution of alloying elements – principally Mg and Mn, per chemical analysis. A strong {200} texture in the solid solution is observed, consistent with elongated α-phase grains and attributable to sheet processing via rolling. The diffraction pattern also shows weak, near-background reflections of secondary Al_3Mg_2 (β-phase) and Al_6Mn phases, present as dispersed inclusions at grain boundaries and within α-phase grains.

3.2 Analysis of the 08Cr18Ni10Ti–AlMg6 weld interface after explosive welding

As a result of EW, a transition layer forms at the AlMg6–08Cr18Ni10Ti weld interface (Fig. 6). The layer thickness varies between 5 and 20 µm. Due to the limited cross-sectional area of the transition layer, the diffraction pattern shows only reflections from the parent phases: the aluminium-based solid solution (α-phase), austenite, and ferrite.

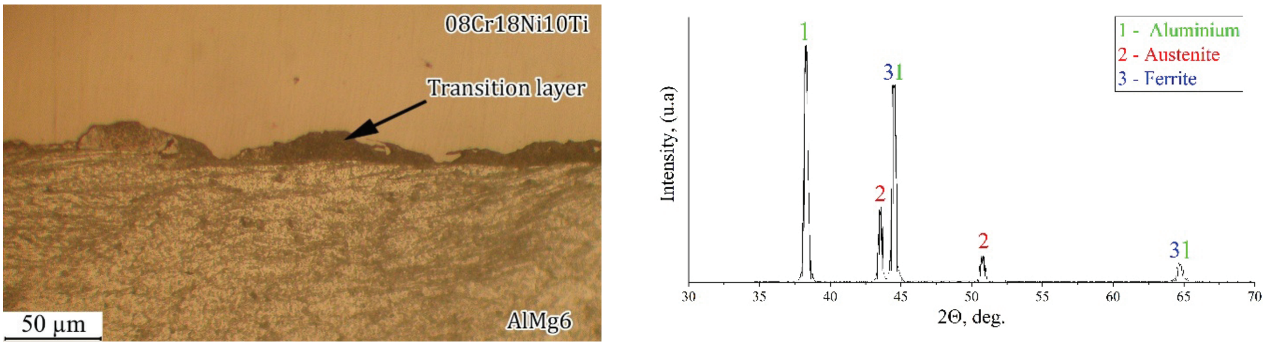

(a) *(b)*

Fig. 6. Explosively welded AlMg6–08Cr18Ni10Ti interface:
a – Transition layer morphology; *b* – XRD pattern showing parent phases only (α-Al, γ-Fe, δ-Fe)

3.2.1. Analysis of the 08Cr18Ni10Ti fracture surface after explosive welding

The diffraction patterns of the 08Cr18Ni10Ti steel specimen after EW shows austenite reflections (Fig. 7). The intensity of the strongest δ-ferrite (110) peak decreases to near-background levels compared to the initial 08Cr18Ni10Ti steel. No new phases were detected at the steel-side weld interface within the detection limits of XRD.

It should be noted that the preferred {220} grain orientation in austenite – initially induced by rolling – is significantly reduced. The relative intensity of the austenite (220) reflection at the welded surface decreases by nearly half (2 times). This indicates recrystallization of austenitic grains in the weld interface region, likely induced by heat exposure and severe plastic deformation during EW. The heat exposure is caused by both plastic deformation and the impact of shock-compressed gas in the welding gap [30]. After removing a ~15 μm surface layer, the intensity of the austenite (220) reflection increases, demonstrating that recrystallization is localized to areas affected by shock loading.

The angular positions of austenite reflections remain identical before and after EW, indicating no change in its lattice parameter. This demonstrates the absence of significant dissolved aluminium in the austenitic phase within the 08Cr18Ni10Ti-side transition layer. It suggests that either no solid solution of Al forms in austenite, or its concentration is insufficient to alter the austenite lattice parameter. Notably, α-phase reflections (FCC Al-based solid solution) appear after removing a 15 μm layer from the 08Cr18Ni10Ti surface, despite this phase being absent at the immediate weld interface. Furthermore, a weak reflection of the $Al_{86}Fe_{14}$ quasi-crystalline phase emerges after the first layer removal – a phase later identified in the surface layer of the AlMg6 alloy post-welding.

The appearance of aluminium-based phases suggests material transfer of AlMg6 alloy grains into the 08Cr18Ni10Ti steel subsurface layer. It should be noted that the angular positions of several diffraction peaks for the α-phase (FCC structure) and ferrite (BCC structure) nearly coincide. Consequently, based on the obtained data, the presence of ferrite in the 08Cr18Ni10Ti surface layer after explosive welding cannot be confirmed. Thus, the primary phase in the steel's surface layer remains austenite, alongside phases transferred from the AlMg6 alloy during shock loading.

3.2.2. Analysis of the AlMg6 alloy fracture surfaces after explosive welding

Thus, this study demonstrates substantial phase transformation in the AlMg6 surface layer following EW. The diffraction patterns (Fig. 8) reveal not only reflections from the original α-phase but also two new phases: an FCC iron-based solid solution (γ-phase) and metastable icosahedral $Al_{86}Fe_{14}$. Removal of a 15 μm layer does not significantly reduce the intensity of these phases. The angular positions of γ-phase reflections match those of 08Cr18Ni10Ti steel's austenite, confirming austenite grain transfer into the AlMg6 surface during welding.

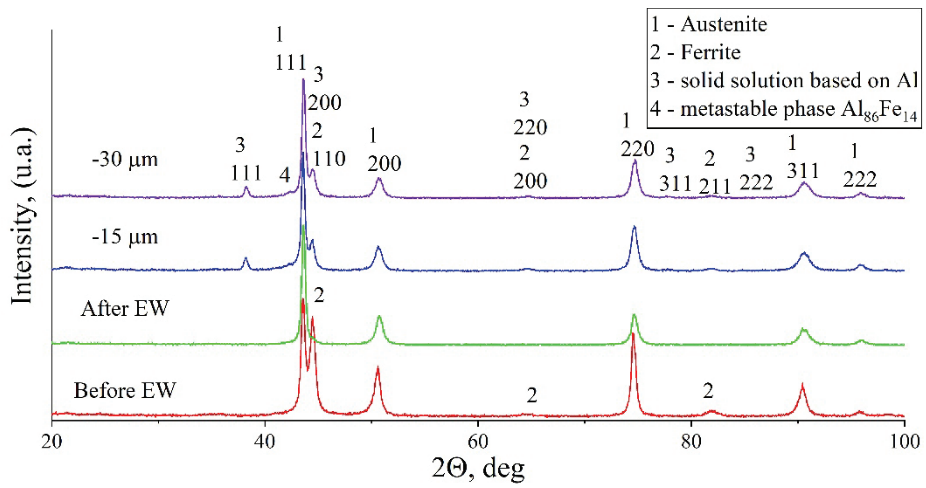

Fig. 7. XRD patterns of the 08Cr18Ni10Ti steel before and after explosive welding

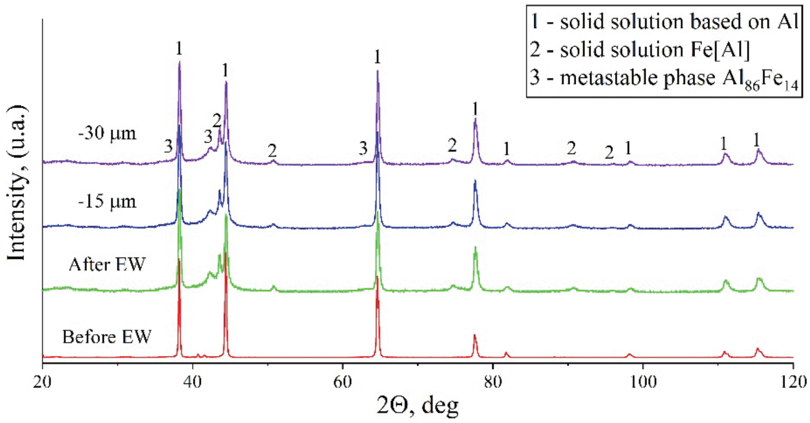

Fig. 8. XRD patterns of the AlMg6 surface before and after explosive welding

The metastable $Al_{86}Fe_{14}$ phase – previously reported by [31] – forms through rapid solidification ($2{\cdot}10^6$ $K{\cdot}s^{-1}$) of Fe–Al melt. It features an icosahedral quasicrystalline structure lacking Bravais lattice periodicity. Notably, its diffraction peaks exhibit significant broadening, indicating nanocrystalline grain size (< 50 nm).

Heating would inevitably decompose the metastable $Al_{86}Fe_{14}$ phase. The differential thermal analysis in [31] demonstrated decomposition at 400 °C via $Al_{86}Fe_{14} \rightarrow Al_6Fe + Al$, followed by further transformation $Al_6Fe \rightarrow Al_3Fe + Al$ at ~530 °C. Thus, the altered phase composition in the AlMg6 surface layer results directly from shock-induced iron transfer from 08Cr18Ni10Ti steel during EW.

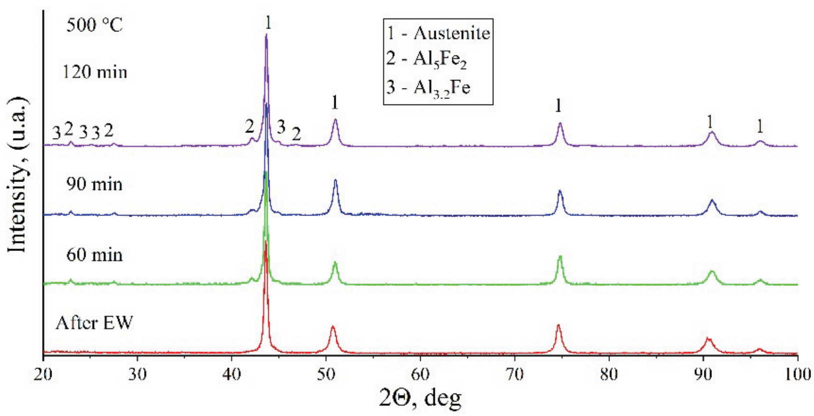

(a)

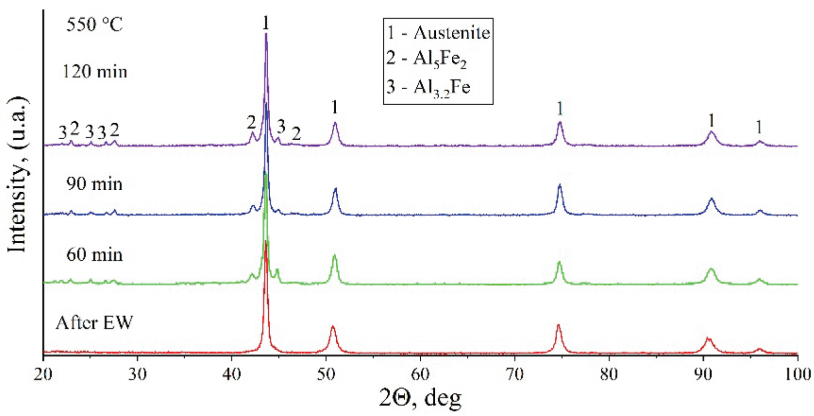

(b)

Fig. 9. XRD patterns of the 08Cr18Ni10Ti steel surface after explosive welding and isothermal annealing:
a – 500 °C; *b* – 550 °C

3.3. Analysis of specimens after explosive welding and isothermal annealing at 500 and 550 °C

3.3.1. Analysis of the 08Cr18Ni10Ti steel surfaces after explosive welding and isothermal annealing at 500 and 550 °C for 60, 90, and 120 minutes

Isothermal annealing of explosively welded AlMg6–08Cr18Ni10Ti specimens at 500–550 °C for 60–120 min alters the phase composition in the steel interfacial region adjacent to AlMg6. Diffraction patterns (Figs. 9*a*, 9*b*) reveal reflections of two iron aluminides – Al_5Fe_2 and $Al_{3.2}Fe$ – alongside the dominant austenite phase. Intermetallic peak intensities increase with higher temperatures and longer durations. Given the absence of new phases at the steel interface in the as-welded state, these transformations confirm post-heating aluminium diffusion into the steel substrate and subsequent formation of iron aluminides upon cooling.

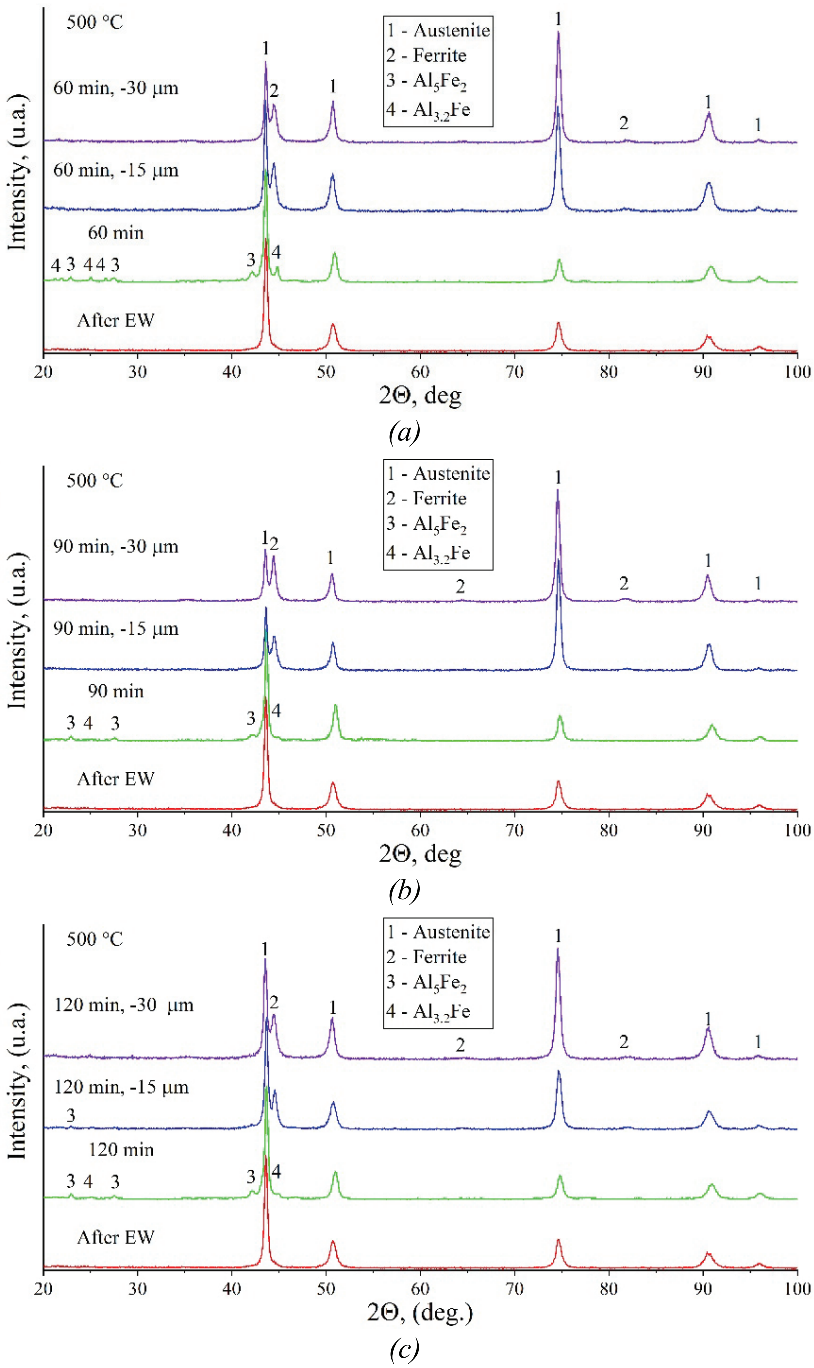

Fig. 10. XRD patterns of the 08Cr18Ni10Ti steel surface after explosive welding, isothermal annealing (at 500 °C), and surface layer removal for: *a* – 60 min; *b* – 90 min; *c* – 120 min

The layer-by-layer XRD analysis of the 08Cr18Ni10Ti steel surface confirms that removing a 15 μm layer eliminates reflections from iron aluminides formed during 500 °C annealing for 60–90 min (Figs. 10*a*, 10*b*). Reflections of α-phase (Al-based) and $Al_{86}Fe_{14}$ – previously detected in the steel subsurface after EW – also disappear. Critically, post-anneal diffraction patterns after 15 μm removal lack the characteristic α-phase (111) reflection at 2θ ≈ 38.5°, which was prominent in the as-welded subsurface layer. This demonstrates that annealing dissolves aluminide phases through aluminium diffusion into austenite and ferrite solid solutions. For 120-minute treatments, aluminium penetration depth increases significantly: iron aluminide reflections persist until removal of a second steel layer (Fig. 10*c*).

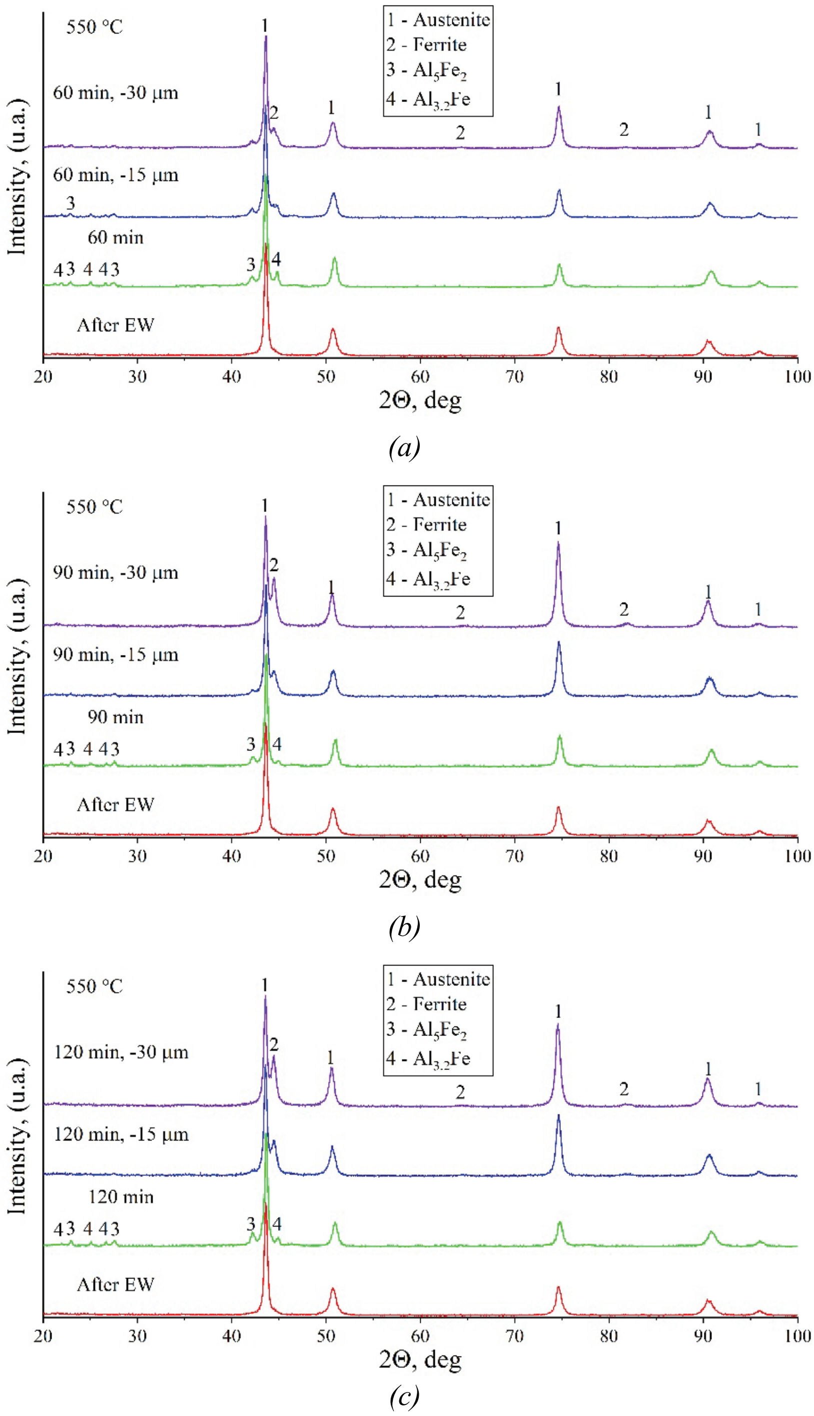

Fig. 11. XRD patterns of the 08Cr18Ni10Ti steel surface after explosive welding, isothermal annealing (at 550 °C), and surface layer removal for: *a* – 60 min; *b* – 90 min; *c* – 120 min

An identical trend occurs at 550 °C heat treatment (Figs. 11*a*, 11*b*). Iron aluminide reflections virtually disappear after 30μm layer removal for both 60- and 90-minute annealed samples. Layer-by-layer analysis further reveals that material removal progressively increases ferrite reflection intensity. After grinding away 30 μm, the intensity matches the pre-welding state of 08Cr18Ni10Ti steel (Fig. 11*c*). The preferred {220} grain orientation in the bulk 08Cr18Ni10Ti steel persists after 500 and 550 °C heat treatments. Consistent with this, removing 30 μm of material increases the intensity of the austenite (220) reflection (Figs. 10 and 11).

Thus, recrystallization of austenitic grains occurs exclusively at the weld interface region, driven by localized heating to high temperatures at the contact zone between 08Cr18Ni10Ti steel and AlMg6 alloy sheets following shock loading.

3.3.2. Analysis of AlMg6 alloy surfaces after explosive welding and isothermal annealing at 500 and 550 °C for 60, 90, and 120 minutes

Isothermal annealing of explosively welded AlMg6–08Cr18Ni10Ti samples at 500–550 °C for 60–120 min alters the phase composition in the AlMg6 interfacial region adjacent to the steel. Diffraction patterns (Fig. 12) reveal reflections of intermetallic phases Al_5Fe_2 and $Al_{13}Fe_4$ – previously identified in the steel interfacial layer after annealing-alongside the primary α-phase (FCC Al-based solid solution). Additionally, reflections of the ternary phase $Cr_2Mg_3Al_{18}$ are observed. This confirms that heating to 500 °C decomposes the metastable quasicrystalline $Al_{86}Fe_{14}$ phase formed in the AlMg6 surface layer during EW, resulting in crystalline iron aluminides Al_5Fe_2 and $Al_{13}Fe_4$. This transformation aligns with prior differential thermal analysis (DTA) study [1], where $Al_{86}Fe_{14}$ (produced by rapid Fe-Al melt quenching) decomposed at ~530 °C. Formation of the $Cr_2Mg_3Al_{18}$ ternary phase during annealing indicates chromium diffusion – a primary alloying element in 08Cr18Ni10Ti steel – into the AlMg6 surface layer, where it reacts with β-phase (Al_3Mg_2) present in the alloy. Intermetallic peak intensities increase with higher temperatures and longer durations.

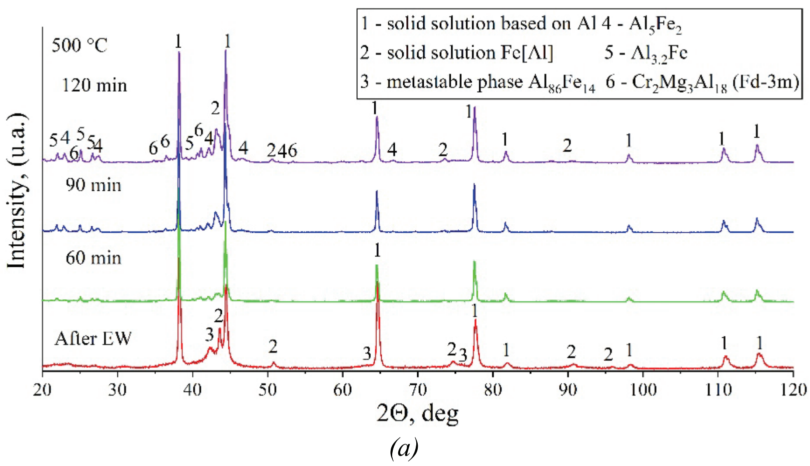

(b)

Fig. 12. XRD patterns of the AlMg6 alloy surface after explosive welding and isothermal annealing for 60, 90, and 120 min at: *a* – 500 °C; *b* – 550 °C

The layer-by-layer XRD analysis of the AlMg6 alloy surface reveals that removing 14–42 µm of material does not fully eliminate intermetallic reflections formed during 500 °C (Fig. 13) and 550 °C (Fig. 14) annealing for 60–120 min. The thickness of the aluminide-containing layer increases with prolonged annealing. Consequently, even after grinding away two layers (~30 µm) from the AlMg6 surface, reflections from Al_5Fe_2, $Al_{13}Fe_4$, and $Cr_2Mg_3Al_{18}$ retain significant intensity. Thus, the explosive-welding-modified layer depth is greater in AlMg6 alloy than in 08Cr18Ni10Ti steel, attributable to localized melting of the AlMg6 surface. The presence of a liquid phase – where bulk diffusion coefficients exceed solid-state values by 4–5 orders of magnitude – enables dissolution of iron and alloying elements from the steel into the molten AlMg6 layer, followed by formation of aluminium-based intermetallic phases (Fig. 14).

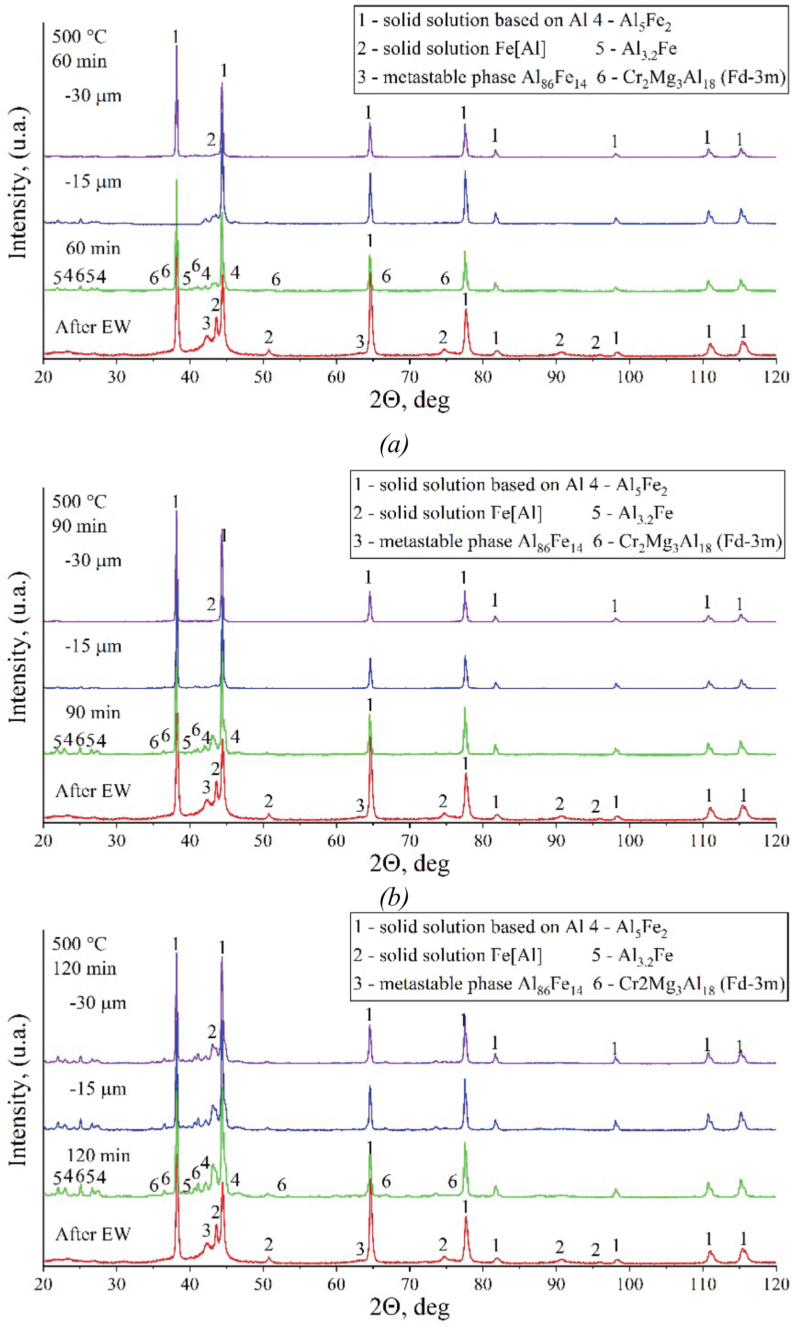

Fig. 13. XRD patterns of the AlMg6 surface after explosive welding, isothermal annealing (at 500 °C), and surface layer removal for: *a* – 60 min; *b* – 90 min; *c* – 120 min

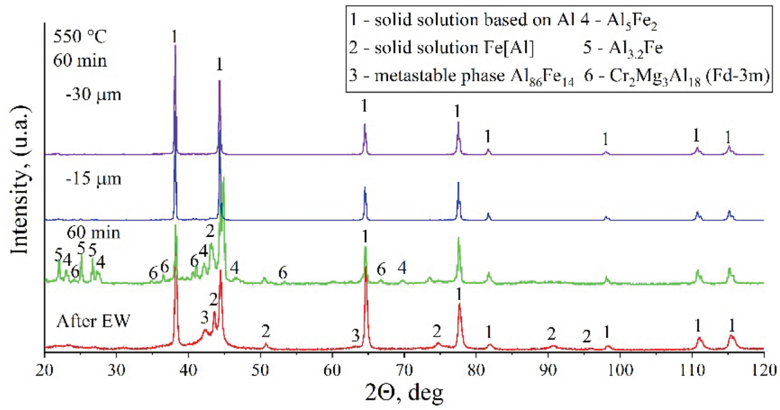

(a)

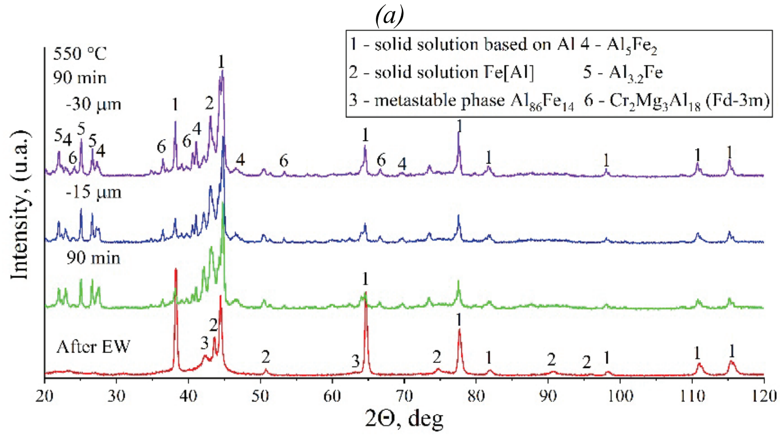

(b)

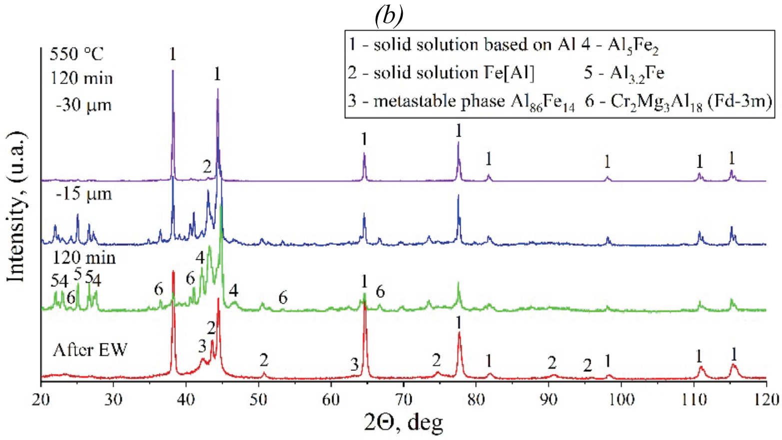

(c)

Fig. 14. XRD patterns of the AlMg6 surface after explosive welding, isothermal annealing (at 550 °C), and surface layer removal for: *a* – 60 min; *b* – 90 min; *c* – 120 min

4. Conclusion

The observed recrystallization of austenitic grains in 08Cr18Ni10Ti steel near the weld interface is determined by the combined effect of plastic deformation and localized heating during explosive welding. The presence of the α-phase and the quasicrystalline $Al_{86}Fe_{14}$ phase in the subsurface layer of 08Cr18Ni10Ti steel after removing a 15 μm-thick layer indicates the transfer of aluminium from the AlMg6 alloy. This process likely occurs due to mechanical mixing and localized melting, promoting the formation of new phases. In the surface layer of the AlMg6 alloy after explosive welding, changes in the phase composition are observed, associated with the transfer of iron from 08Cr18Ni10Ti steel. This leads to the formation of an FCC iron-based solid solution (γ-phase) and the metastable icosahedral $Al_{86}Fe_{14}$ phase.

Isothermal annealing of the bimetallic sample results in the diffusion of aluminium deeper into the steel and the subsequent formation of iron aluminides upon cooling. It is evident that annealing leads to the dissolution of aluminide phases, forming solid solutions of aluminium in austenite and ferrite. Thus, it is clear that the recrystallization of austenitic grains occurs only in the weld interface region and is associated with localized heating to high temperatures in the contact zone of 08Cr18Ni10Ti steel and AlMg6 alloy plates after exposure to plastic deformation and shock-compressed gas. The layer-by-layer XRD analysis revealed that the removal of material layers leads to an increase in the intensity of ferrite reflections. After removing a 30 μm-thick layer, the reflection intensity reaches values characteristic of the material's initial state before explosive welding. This indicates that the top layer, subjected to the most intense impact during welding, contains structural changes that can be eliminated by removing a thin surface layer. The restoration of the initial ferrite characteristics after removing 30 μm confirms that these changes are localized in the surface zone and do not affect the deeper material layers. The findings extend the current understanding of the mechanisms governing phase formation and diffusion processes during explosive welding, and also shed light on the effect of thermal exposure on phase evolution.

5. Funding

This work was supported by Russian Science Foundation No. 23-19-00446, https://rscf.ru/project/23-19-00446/

Финансирование

Исследование выполнено за счет средств гранта Российского научного фонда № 23-19-00446, https://rscf.ru/project/23-19-00446/

6. Acknowledgements

This research was performed by using the set of modern scientific instruments available for multiple accesses at the ISMAN Center of Shared Services.

Благодарности

Данное исследование было проведено с применением комплекса современных научных приборов на базе Центра коллективного пользования ИСМАН.

7. Conflict of interests

The authors declare no conflict of interest.

Конфликт интересов

Авторы заявляют об отсутствии конфликта интересов.

References

1. Starke EA, Rashed HMMA. Alloys: aluminum. In: *Reference Module in Materials Science and Materials Engineering*. Elsevier; 2017. DOI:10.1016/B978-0-12-803581-8.09210-9

2. Pesin AM, Pustovoytov DO, Steblyanko VL, Fedoseev SA. Physical and computer simulation of severe plastic deformations on shear-compression testing of AMg6 (АМг6) aluminium alloy. *Non-Ferrous Metals*. 2017;42(1):17-21. DOI:10.17580/nfm.2017.01.04

3. Wahid MA, Siddiquee AN, Khan ZA. Aluminum alloys in marine construction: characteristics, application, and problems from a fabrication viewpoint. *Marine Systems & Ocean Technology*. 2020;15(1):70-80. DOI:10.1007/s40868-019-00069-w

4. Yang J, Li Y long, Zhang H. Microstructure and mechanical properties of pulsed laser welded Al/steel dissimilar joint. *Transactions of Nonferrous Metals Society of China*. 2016;26(4):994-1002. DOI:10.1016/S1003-6326(16)64196-1

5. Moreno-Blanco J, Petitpas G, Espinosa-Loza F, Elizalde-Blancas F, et al. The fill density of automotive cryo-compressed hydrogen vessels. *International Journal of Hydrogen Energy*. 2019;44(2):1010-1020. DOI:10.1016/j.ijhydene.2018.10.227

6. Agudo L, Eyidi D, Schmaranzer CH, Arenholz E, et al. Intermetallic Fe_xAl_y-phases in a steel/Al-alloy fusion weld. *Journal of Materials Science*. 2007;42(12):4205-4214. DOI:10.1007/s10853-006-0644-0

7. Rathod MJ, Kutsuna M. Joining of aluminum Alloy 5052 and low-carbon steel by laser roll welding. *Welding Journal*. 2004;83(1):16-26.

8. Shubhavardhan RN, Surendran S. Friction welding to join stainless steel and aluminum materials. *International Journal of Metallurgical & Materials Science and Engineering*. 2012;2:53-73.

9. Tsujino J, Hidai K, Hasegawa A, Kanai R, et al. Ultrasonic butt welding of aluminum, aluminum alloy and stainlesssteel plate specimens. *Ultrasonics*. 2002;40(1-8): 371-374. DOI:10.1016/S0041-624X(02)00124-5

10. Acarer M, Demir B. An investigation of mechanical and metallurgical properties of explosive welded aluminum-dual phase steel. *Materials Letters*. 2008;62(25):4158-4160. DOI:10.1016/j.matlet.2008.05.060

11. Sierra G, Peyre P, Deschaux-Beaume F, Stuart D, et al. Steel to aluminium key-hole laser welding. *Materials Science and Engineering: A*. 2007;447(1-2):197-208. DOI:10.1016/j.msea.2006.10.106

12. Bugajska M, Maj L, Jarzebska A, Terlicka S, et al. Variety of aluminum/steel interface microstructures formed in explosively welded clads followed by the weld's thermal expansion response. *Journal of Materials Engineering and Performance*. 2022;31(9):7088-7097. DOI:10.1007/s11665-022-07027-5

13. He P, Yue X, Zhang JH. Hot pressing diffusion bonding of a titanium alloy to a stainless steel with an aluminum alloy interlayer. *Materials Science and*

Engineering: A. 2008;486(1-2):171-176. DOI:10.1016/j.msea.2007.08.076

14. Giudice F, Missori S, Scolaro C, Sili A. A review on metallurgical issues in the production and welding processes of clad steels. *Materials*. 2024;17(17):4420. DOI:10.3390/ma17174420

15. Schubert E, Klassen M, Zerner I, Walz C, et al. Light-weight structures produced by laser beam joining for future applications in automobile and aerospace industry. *Journal of Materials Processing Technology*. 2001;115(1):2-8. DOI:10.1016/S0924-0136(01)00756-7

16. Chen X, Inao D, Tanaka S, Mori A, et al. Explosive welding of Al alloys and high strength duplex stainless steel by controlling energetic conditions. *Journal of Manufacturing Processes*. 2020;58:1318-1333. DOI:10.1016/j.jmapro.2020.09.037

17. Potesser M, Schoeberl T, Antrekowitsch H, Bruckner J. The characterization of the intermetallic Fe–Al layer of steel-aluminum weldings. In: *EPD Congress 2006*, Howard SM et al (eds). TMS; 2016. p. 167-176.

18. Gąsior W, Dębski A, Moser Z. Formation enthalpy of intermetallic phases from Al–Fe system measured with solution calorimetric method. *Intermetallics.* 2012;24:99-105. DOI:10.1016/j.intermet.2012.02.001

19. Shirzadi AA, Zhang C, Mughal MZ, Xia P. Challenges and latest developments in diffusion bonding of high-magnesium aluminium alloy (Al-5056/Al-5A06) to stainless steels. *Metals*. 2022;12(7):1193. DOI:10.3390/met12071193

20. Li B, Han S, Ao W, Yang Y, et al. Investigation on microstructure and mechanical properties of the dissimilar lap welding of Al alloy to steel with different filler materials and laser powers. *The International Journal of Advanced Manufacturing Technology*. 2024;134(1-2):935-948. DOI:10.1007/s00170-024-14185-4

21. Atabaki MM, Nikodinovski M, Chenier P, Ma J, et al. Welding of aluminum alloys to steels: an overview. *Journal for Manufacturing Science and Production*. 2014;14(2):59-78. DOI:10.1515/jmsp-2014-0007

22. Beygi R, Galvão I, Akhavan-Safar A, Pouraliakbar H, et al. Effect of alloying elements on intermetallic formation during friction stir welding of dissimilar metals: a critical review on aluminum/steel. *Metals*. 2023;13(4):768. DOI:10.3390/met13040768

23. Rahman SAA, Mamat S, Ahmad MI, Mungkung N, et al. Study on intermetallic compound (IMC) in dissimilar joining of steel and aluminum (Fe-Al) – a review paper. *Welding in the World*. 2024;68(9):2351-2376. DOI:10.1007/s40194-024-01784-8

24. Aceves SM, Espinosa-Loza F, Elmer JW, Huber R. Comparison of Cu, Ti and Ta interlayer explosively fabricated aluminum to stainless steel transition joints for cryogenic pressurized hydrogen storage. *International Journal of Hydrogen Energy*. 2015;40(3):1490-1503. DOI:10.1016/j.ijhydene.2014.11.038

25. Aizawa Y, Nishiwaki J, Harada Y, Muraishi S, et al. Experimental and numerical analysis of the formation behavior of intermediate layers at explosive welded Al/Fe joint interfaces. *Journal of Manufacturing Processes*. 2016;24:100-106. DOI:10.1016/j.jmapro.2016.08.002

26. Sherpa BB, Rani R. Advancements in explosive welding process for bimetallic material joining: A review. *Journal of Alloys and Metallurgical Systems*. 2024;6:100078. DOI:10.1016/j.jalmes.2024.100078

27. Haidara F, Record MC, Duployer B, Mangelinck D. Phase formation in Al–Fe thin film systems. *Intermetallics*. 2012;23:143-147. DOI:10.1016/j.intermet.2011.11.017

28. Malakhov AY, Saikov IV, Denisov IV, Niyezbekov NN. AlMg6 to titanium and AlMg6 to stainless steel weld interface properties after explosive welding. *Metals*. 2020;10(11):1500. DOI:10.3390/met10111500

29. Lysak VI, Kuzmin SV. Energy balance during explosive welding. *Journal of Materials Processing Technology*. 2015;222:356-364. DOI:10.1016/j.jmatprotec.2015.03.024

30. Malakhov A, Denisov I, Niyozbekov N, Saikov I, et al. Theoretical and experimental studies of the shock-compressed gas parameters in the welding gap. *Materials*. 2024;17(1):265. DOI:10.3390/ma17010265

31. Dunlap RA, Dini K. Formation, structure, and crystallization of metastable quasi-crystalline Al-transition metal alloys prepared by rapid solidification. *Canadian Journal of Physics*. 1985;63(10):1267-1269. DOI:10.1139/p85-208

Information about the authors / Информация об авторах

Andrey Yu. Malakhov, Cand. Sc. (Eng.), Senior Researcher, Merzhanov Institute of Structural Macrokinetics and Materials Science RAS (ISMAN), Chernogolovka, Russian Federation; ORCID 0000-0002-0567-7307; e-mail: sir.malahov2009@yandex.ru

Малахов Андрей Юрьевич, кандидат технических наук, старший научный сотрудник, Институт структурной макрокинетики и проблем материаловедения им. А. Г. Мержанова РАН (ИСМАН), Черноголовка, Российская Федерация; ORCID 0000-0002-0567-7307; e-mail: sir.malahov2009@yandex.ru

Dmitry Yu. Kovalev, D. Sc. (Phys. and Math.), Chief Research, ISMAN, Chernogolovka, Russian Federation; ORCID 0000-0002-8285-5656; e-mail: kovalev@ism.ac.ru

Ковалев Дмитрий Юрьевич, доктор физико-математических наук, главный научный сотрудник, ИСМАН, Черноголовка, Российская Федерация; ORCID 0000-0002-8285-5656; e-mail: kovalev@ism.ac.ru

Stepan A. Seropyan, Junior Research, ISMAN, Chernogolovka, Russian Federation; ORCID 0000-0002-3714-3983; e-mail: stepan.seropyan@yandex.ru

Nemat N. Niyozbekov, Junior Research, ISMAN, Chernogolovka, Russian Federation; ORCID 0000-0003-1812-2930; e-mail: nemat199595@mail.ru

Igor V. Denisov, Cand. Sc. (Eng.), Senior Researcher, ISMAN, Chernogolovka, Russian Federation; ORCID 0000-0002-1065-3318; e-mail: denisov@ism.ac.ru

Gulnaz R. Saikova, Cand. Sc. (Eng.), Senior Researcher, ISMAN, Chernogolovka, Russian Federation; ORCID 0000-0002-6542-7123; e-mail: gulnaz-84@mail.ru

Серопян Степан Арутюнович, младший научный сотрудник, ИСМАН, Черноголовка, Российская Федерация; ORCID 0000-0002-3714-3983; e-mail: stepan.seropyan@yandex.ru

Ниёзбеков Неъмат Ниёзбекович, младший научный сотрудник, ИСМАН, Черноголовка, Российская Федерация; ORCID 0000-0003-1812-2930; e-mail: nemat199595@mail.ru

Денисов Игорь Владимирович, кандидат технических наук, старший научный сотрудник, ИСМАН, Черноголовка, Российская Федерация; ORCID 0000-0002-1065-3318; e-mail: denisov@ism.ac.ru

Сайкова Гульназ Рафиковна, кандидат технических наук, старший научный сотрудник, ИСМАН, Черноголовка, Российская Федерация; ORCID 0000-0002-6542-7123; e-mail: gulnaz-84@mail.ru

Received 29 October 2025; Revised 28 November 2025; Accepted 03 December 2025